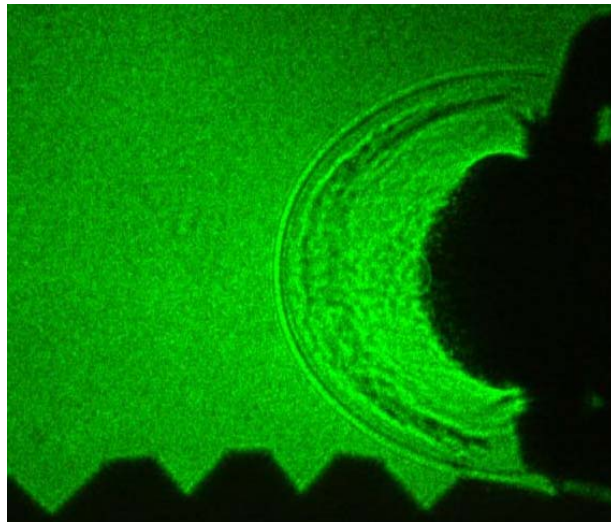


Characterization of the Absorption Wave Produced by CO₂ Laser Ablation of a Solid Propellant

**EOARD Grant
Award No. FA8655-04-1-3067**

**Final Report
October 2005**



Project Officer: Wolfgang O. Schall

Co-authors: Hans-Albert Eckel, Jochen Tegel, Frank Holzschuh

**DLR- German Aerospace Center
Institute of Technical Physics
Pfaffenwaldring 38 – 40
D-70569 Stuttgart
Germany**

Report Documentation Page

*Form Approved
OMB No. 0704-0188*

Public reporting burden for the collection of information is estimated to average 1 hour per response, including the time for reviewing instructions, searching existing data sources, gathering and maintaining the data needed, and completing and reviewing the collection of information. Send comments regarding this burden estimate or any other aspect of this collection of information, including suggestions for reducing this burden, to Washington Headquarters Services, Directorate for Information Operations and Reports, 1215 Jefferson Davis Highway, Suite 1204, Arlington VA 22202-4302. Respondents should be aware that notwithstanding any other provision of law, no person shall be subject to a penalty for failing to comply with a collection of information if it does not display a currently valid OMB control number.

| | | | |
|--|------------------------------------|--|----------------------------------|
| 1. REPORT DATE 25 APR 2005 | 2. REPORT TYPE N/A | 3. DATES COVERED | |
| 4. TITLE AND SUBTITLE Characterization of the Absorption Wave Produced by CO2 Laser Ablation of a Solid Propellant | | 5a. CONTRACT NUMBER | |
| | | 5b. GRANT NUMBER | |
| | | 5c. PROGRAM ELEMENT NUMBER | |
| 6. AUTHOR(S) | | 5d. PROJECT NUMBER | |
| | | 5e. TASK NUMBER | |
| | | 5f. WORK UNIT NUMBER | |
| 7. PERFORMING ORGANIZATION NAME(S) AND ADDRESS(ES) German Aerospace Center (DLR) Pfaffenwaldring 38-40 Stuttgart D-70569 Germany | | 8. PERFORMING ORGANIZATION REPORT NUMBER | |
| 9. SPONSORING/MONITORING AGENCY NAME(S) AND ADDRESS(ES) | | 10. SPONSOR/MONITOR'S ACRONYM(S) | |
| | | 11. SPONSOR/MONITOR'S REPORT NUMBER(S) | |
| 12. DISTRIBUTION/AVAILABILITY STATEMENT Approved for public release, distribution unlimited. | | | |
| 13. SUPPLEMENTARY NOTES The original document contains color images. | | | |
| 14. ABSTRACT | | | |
| 15. SUBJECT TERMS | | | |
| 16. SECURITY CLASSIFICATION OF: | | | 17. LIMITATION OF ABSTRACT |
| a. REPORT unclassified | b. ABSTRACT unclassified | c. THIS PAGE unclassified | UU |
| | | | 18. NUMBER OF PAGES 38 |
| | | | 19a. NAME OF RESPONSIBLE PERSON |

The contractor, German Aerospace Center (DLR), Institute of Technical Physics, hereby declares that, to the best of its knowledge and belief, the technical data delivered herewith under Contract No: FA8655-04-1-3067 is complete, accurate, and complies with all requirements of the contract.

Stuttgart, October 2005



Prof. W. L. Bohn
Director
Institute of Technical Physics

I certify that there were no subject inventions to declare as defined in FAR 52.227-13, during the performance of this contract.

Stuttgart, October 2005



Prof. W. L. Bohn
Director
Institute of Technical Physics

SUMMARY

Characterization of the Absorption Wave Produced by CO₂ Laser Ablation of a Solid Propellant

A requirement for efficient pulsed laser propulsion from ground to LEO is the achievement of a specific impulse of up to 800 s at a jet efficiency of at least 50%. With CO₂ laser radiation at pulse lengths in the range of 10 microseconds and polymers as propellant these numbers cannot be attained by classical laser ablation. Also the blending of the polymers with various metal powders did not improve the situation. Obviously the major reason for the impossibility to deposit enough energy in a sufficiently small volume are severe absorption losses in gases building up during the laser pulse in front of the target surface. Energy, that is dissipated in this region, does not improve the generation of a pressure force on the target and is therefore lost for thrust production.

It was the aim of this research to get firstly an idea of the losses as a function of the incident energy, the environmental conditions (standard pressure air or vacuum), and the ablated material (POM with and without metal content). Secondly, the expansion of the ablation products and the build-up and spreading of the absorption zone in front of the propellant surface have been observed.

For the first task the laser power fraction penetrating through the absorption region towards the target surface and escaping through a small hole in the target to the rear was measured. The power was picked up by a fast powermeter and compared with the shape of the emitted power curve. It was found that the transmitted energy fraction is directly proportional to the inverse of the pulse energy.

The expansion of the ablation plasma was observed by a Schlieren technique in the light of a frequency doubled pulsed Nd:YAG laser at various time delays after the beginning of the CO₂ laser pulse. The fluence at the target was set to 13, 37, and 75 J/cm² and the pressure to below 0.5 mbar (< 50 Pa) and also to 35 mbar in order to observe the generation of a shock wave. A plasma can be seen to expand with an initial velocity of 2 km/s for the lowest fluence and increasing to 2.5 km/s for the highest. The maximum extension of the plasma is about 1 cm. A remarkable observation is the explosive expulsion of matter from POM blended with 20% of aluminum powder. The expulsion is delayed by approximately 2 μs and the velocity of the

products can reach over 8 km/s. The ejected material literally breaks through the shock wave which was released at the beginning of the laser pulse. Surprisingly, this process does not enhance the coupling coefficient.

Finally, the development and extension of the absorption region was monitored by sending CO₂ probe laser beams parallel to the target surface across the absorption zone. The distance of the probe beam from the target surface was varied between 3 mm and 24 mm and the development of the power profile due to absorption was measured by fast powermeters. The front of the absorption zone is found to move rapidly away from the target surface with increasing speed. The absorption lasts twice as long as the laser pulse. It is not associated with a pressure rise that would increase the mechanical impulse. The radial motion of the absorption wave turned out to be faster than the shock wave seen in the Schlieren pictures. The question for the media that produces the absorption could not be answered. In some cases, absorption sets in within a microsecond after the start of the laser pulse even out to a distance of at least 16 mm. This effect could not be connected with any particular process.

The experiments led to the conclusion that the applied laser pulse length in the range of 10 to 15 μ s is either much too long or too short. A pulse length of several hundred nanoseconds could possibly prevent the appearance of an extended absorbing material cloud before the incident laser pulse is terminated. On the other hand, the placement of the ablation zone in some kind of thrust chamber can lead to a pressure rise in the outflowing vapor by utilizing the absorbing energy for increasing the thrust. In addition, a lower intensity would increase the energy fraction arriving at the target.

Characterization of the Absorption Wave Produced by CO₂ Laser Ablation of a Solid Propellant

| | |
|--|-----------|
| 1. INTRODUCTION | 8 |
| 1.1 Purpose of the project | 8 |
| 1.2 Background | 8 |
| 1.3 Technical approach and methodology | 9 |
| 2. EXPERIMENTAL SETUP AND INSTRUMENTATION | 11 |
| 2.1 Schlieren photography | 11 |
| 2.2 Time dependent absorption measurement | 13 |
| 3. RESULTS AND INTERPRETATION | 16 |
| 3.1 Energy absorption | 16 |
| 3.2 Schlieren photography | 19 |
| 3.3 Velocity of the ablation products | 21 |
| 3.4 Results of the absorption measurements | 26 |
| 3.5 Abnormal absorption | 32 |
| 4. CONCLUSION | 35 |

Acknowledgements

Literature

Appendix A

Appendix B

LIST OF FIGURES

Front page: Schlieren picture of expanding plasma and shock wave in low pressure air

Fig. 1: Setup for the Schlieren Photography

Fig. 2: Trigger procedure for the Schlieren photography

Fig. 3: Initial Setup for the absorption measurement with 4 probe beams

Fig. 4: Fraction of energy transmitted to the target surface

Fig. 5: Correlation of the energy transmission ratio with the incident pulse energy

Fig. 6: Length of laser pulse transmitted to the target surface

Fig. 7: Comparison of extrapolated potential coupling coefficients for suppressed absorption with actually measured values

Fig. 8: Space/time diagram of the shock and contact front for a pulse energy of 25 J in comparison with the intensity curve. Target material: POM

Fig. 9: Space/time diagram of the shock and contact front for a pulse energy of 75 J in comparison with the intensity curve. Target material: POM

Fig. 10: Space/time diagram of the shock and contact front for a pulse energy of 150 J in comparison with the intensity curve. Target material: POM

Fig. 11: Space/time diagram of the shock and contact front for a pulse energy of 75 J in comparison with the intensity curve. Target material: POM + 20% Al and PVN

Fig. 12: Space/time diagram of the shock and contact front for a pulse energy of 150 J in comparison with the intensity curve. Target material: POM + 20% Al

Fig. 13: Temporal development of the CO₂ wavelength absorption at various distances from target surface for a pulse energy of 150 J

Fig. 14: 3-dimensional representation of the absorption wave

Fig. 15: Time of the onset and the maximum of the absorption

Fig. 16: Velocities of the absorption wave

Fig. 17: Temporal development of the absorption wave, when a low pressure background gas (air at 30 mbar) is present

Fig. 18: Temporal behavior of the absorption in vacuum for a pulse energy of 75 J

Fig. 19: Time of the onset of absorption for different conditions

Fig. 20: Spreading velocity of the absorption wave

Fig. 21: Comparison of the abnormal absorption with the regular case

Fig. 22: Comparison of normal and abnormal absorption curves for different experimental conditions

1. INTRODUCTION

1.1 Purpose of the project

The primary objective of this research is to enable control of the properties of gases that are produced by ablation of a solid polymer (i.e. Delrin = POM) with a pulsed CO₂ laser. Target gas properties of (1) a specific energy content greater than 100 MJ/kg, (2) a specific impulse range from 200 to 800 seconds, and (3) an overall efficiency of jet kinetic energy to laser energy of at least 50% have not been met in previous experiments. Apparently not all of the incident energy can be deposited in the target material. An understanding is required of the mechanisms that hamper the deposition of the full laser pulse energy. Purpose of this project is to investigate and characterize the development of the absorbing region in vacuum as a function of the incident pulse energy for typical pulse durations of 12 to 15 μs. An understanding of the underlying physics may help to control or even utilize the absorption process for the achievement of higher coupling coefficients.

1.2 Background

The efficiency of the ablation of solid polymers for the production of impulses under various conditions has been studied intensively for CO₂ laser pulses of pulse lengths between 12 and 15 μs. Flat samples have been irradiated with fluence values (incident energy per unit area) ranging from 22 to 150 J/cm² and with intensities on the target from 2 to 15 MW/cm² (Ref. 1). The values cover the region designated optimum for the attainable coupling coefficient (defined as impulse exerted per Joule of laser pulse energy) (Ref. 2). Measurements of the laser power arriving on the sample surface as a function of the incident laser pulse energy have indicated severe energy losses in front of the target. The source for these losses not only reduces the arriving energy in magnitude but also shortens the length of the effective pulse on the target surface (Ref. 1). It is well known, that in experiments with pulsed laser ablation a breakdown of the air or of ablated material in front of the target occurs by Inverse Bremsstrahlung and launches a laser supported detonation wave that moves away from the surface. In this wave much of the laser pulse energy may be captured, preventing further ablation and hence the production of impulse by conservation of momentum. However, it was impossible to address this question in detail within the scope of the project of ref. 1. The question of the character and motion of the absorbing wave or layer could not be answered with the then available experimental tools. The proof of the existence and the knowledge of

the position of an emerging laser absorption wave in front of the surface is imperative for the understanding of the obvious losses of laser energy. The absorption process may not only be a function of the fluence on the target, but also of the pulse length and hence the intensity. If the pertinent processes are known and understood it may be possible to find solutions for preventing them or turning them into positive action, i.e. by appropriate geometries of the propulsion devices.

The understanding and observation of the on-going processes requires the application of short-time measurement techniques. Beside an application of short-time photography with appropriate visualisation technology at the CO₂ laser wavelength, a simpler and cheaper method is the transection of the region of the vapor and plasma region with one or several CO₂ probe beams in combination with fast detectors. The measurement with beams at various distances from the target surface can render information on the local appearance, the lifetime and the optical thickness of absorbing media at every location and thus detect even moving absorption waves. In combination with a shadowgraphic or Schlieren type of visualization of the flow field, valuable insight should be gained into the prevailing processes and the character of the laser initiated absorption wave.

Measurements of this type may also give hints to the question, if the produced laser power profile in time, with its two peaks of about 5 μ s separation, does simulate a true double pulse effect. The double pulse effect is expected to enhance the total impulse by the following mechanism (Ref. 3): With the first pulse some vapor is liberated from the target surface by ablation and moves away from the surface with approximately thermal velocity. Before the vapor moves too far away from the surface and thins out, a second pulse is placed inside the vapor cloud. The ensuing laser detonation wave expands spherically and exerts an additional impulse component to the target when hitting its surface.

1.3 Technical approach and methodology

The experiments were carried out at the same teststand as the experiments in the previous investigations. A CO₂ laser pulse of 12 to 15 μ s in duration and with various energies was slightly focussed and directed on flat samples of POM. The power profile of the laser pulse was monitored by fast powermeters. The gaining of insight into the absorption problem was then approached by 3 independent methods:

- 1) Measurement of the profile of the pulse power transmitted through the absorbing region and through a small hole in the sample target as a function of pulse energy. The measurements were carried out with different materials in environmental air and in vacuum.
- 2) Produce shadow or Schlieren pictures of the expanding gas/plasma in the visible with exposure times much shorter than the characteristic expansion time. Pictures with varying delay after the laser pulse ignition allow to observe the development of the expanding material cloud and to measure directly its velocity. The measurements were carried out with different pulse energies in vacuum and in low pressure air. The pressure was kept so low that the expansion was not decelerated by the counter pressure. But it was kept high enough so that the released shock wave in the surrounding medium could be seen and followed.
- 3) Measure the absorption of a CO₂ laser probe beam across and parallel to the target surface as a function of time and distance from the surface. The measurements were carried out in vacuum for 2 extreme pulse energies and at the same pressure of ambient air as for the Schlieren pictures for a direct comparison.

2. EXPERIMENTAL SETUP AND INSTRUMENTATION

The arrangement of the CO₂ pulse laser and the measurement of pulse energy and power has been described in previous reports, including the measurement setup for the power transmitted through a 3 mm diameter hole in the target samples (ref. 1). With a few exceptions of PVN, the sample material was in all cases either plain POM or POM with 20% of aluminum powder, as used in previous investigations. A few samples of PVN with different additives were delivered by Th. Lippert (Paul Scherrer Institut, Switzerland). These samples were thin films, fixed on a substrate. The samples could not sustain more than 3 pulses each.

The laser beam was focused onto the sample surface at 1.2 m distance from a spherical copper mirror with 2 m radius of curvature. The diameter of the laser beam on the flat samples was 15.5 mm. The pulse energy was varied by the change of the laser energy itself or, additionally, by placing a calibrated wire mesh in the laser beam. The samples were positioned in a vacuum tank.

2.1 Schlieren photography

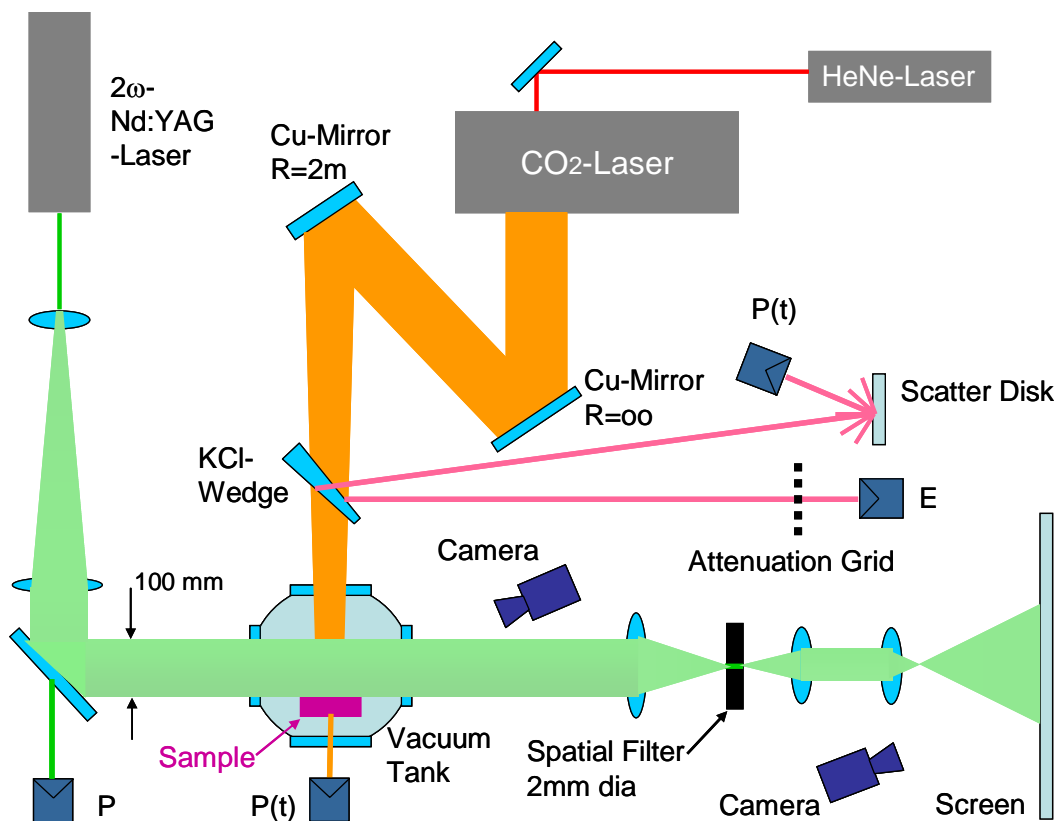


Fig. 1: Setup for the Schlieren Photography

The setup for the Schlieren pictures is illustrated in **fig. 1**. The pulsed light source consisted of a frequency doubled Nd:YAG laser (wavelength 532 nm) with a pulse length of 5-7 ns. The beam diameter was enlarged by a simple lens telescope to a diameter of 10 cm and sent through optical ports into the vacuum tank. The light passed across the sample parallel to its surface and out of the tank on the opposite side. There it was refocused and sent through a 2 mm diameter orifice. The orifice not only cleaned up the picture from speckles, but also removed reflexes from beams bent in the density gradient field of the expanding ablation products. The insertion of a knife edge, as conventional for Schlieren photography, did not improve the picture and was therefore not used. The orifice replaced the knife edge in this fully 3-dimensional expansion. The expanding green laser beam was projected on a white paper screen and photographed from there with a digital camera. Problems with matching the intensity to the sensitivity of the camera were removed with this procedure. A disadvantage of the camera setup was the oblique viewing angle and some pillow type distortions of the picture. The field of view had a diameter of 80 mm. The problem of quantitative length measurements in this non-flat picturing was mediated by placing a saw tooth type scale underneath the sample with kerves every ten millimeters. A scale correction in the plane parallel to the sample surface was not attempted.

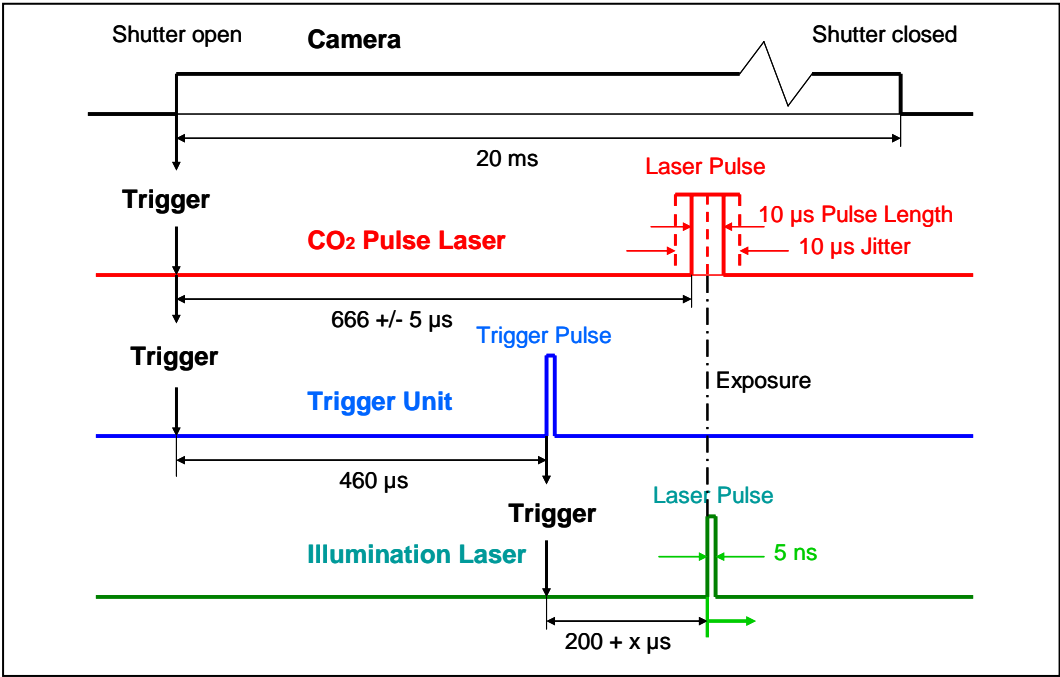


Fig. 2: Trigger procedure for the Schlieren photography

For catching frames of the whole expansion process, the illumination laser was triggered by the camera and delayed via a trigger unit by 200 μs plus various time steps of up to 25 μs from the beginning of the CO_2 laser pulse. The trigger sequence is shown in **fig. 2**. The trigger pulse from the camera also starts the pulse of the CO_2 laser, which comes with a natural delay of about 670 μs and a jitter of approximately 10 μs . The trigger unit allowed to delay the firing of the illumination laser such that it matched with the desired time after the start of the ablation process. The jitter of both lasers made it necessary to produce a sufficient number of pictures with a set time to be able to select those with the actually desired timing.

Since the blown-off material was not dense enough to become visible in the pictures with a vacuum below 1 mbar, an indirect method was chosen to monitor the expansion: The pressure in the tank was raised to approximately 35 mbar. This pressure is expected to be still low enough to be neglected as a counterforce for the expansion process. Nevertheless, the initial ablation motion releases a semi-spherical shock wave into the surrounding air that can be seen in the Schlieren pictures. The velocity of the shock wave can be determined from a sequence of pictures with various time delays. No velocity in the process can be greater than the shock velocity. Otherwise, a new shock wave would be released. Using 1-dimensional shock relations as an approximation, the material velocity (contact front) and the thermodynamic state immediately behind the shock wave can be calculated. It is expected, that the velocity of the contact front is the same as that of the material boundary in vacuum.

2.2 Time dependent absorption measurement

The Schlieren pictures visualized the expansion process of the ablation products in the visible light. If the absorption in the plasma is strong enough it can also be seen. The question is now, where will the CO_2 radiation of the pulse laser be absorbed predominantly? This was attempted to be measured by a time resolved observation of the attenuation of continuous CO_2 laser beams across the expansion zone. Since no picture producing camera for the CO_2 wavelength has been available, only a pointwise absorption measurement was possible. The CO_2 probe laser beam was not expanded but slightly focused by a lens with a long focal length of 500 mm. The focus had a diameter of approximately 2 mm and was placed on the central axes of the expansion cloud. At first it was attempted to split the probe laser beam into 4 individual and parallel beams by semi-transparent mirrors and use 4 independent fast detectors for measuring the timely behavior of the arriving power. However, with a cw power

of the CO₂ probe laser of 1 mW the individual beams were too weak for a discrimination against the infrared background of the plasma radiation. So the idea of using 4 parallel probe beams simultaneously was discarded and instead only 1 beam was used. Beam and detector were translated from shot to shot along the expansion axis. A bending mirror and a focusing lens on one side of the ablation zone and a re-focusing lens for placing the probe beam into the powermeter on the other side were mounted on a common table. So, the whole optic could be moved simultaneously without realignment of the receiver. In the same way as for the Schlieren photography, the probe beams were transmitted through the vacuum tank with the ablation sample. **Fig. 3** is a schematic of the initial setup with 4 beams. The figure is simplified with respect to the beam guidance through the tank and the focusing through the ablation zone. Also omitted is the optical shielding of the detector against indirect radiation.

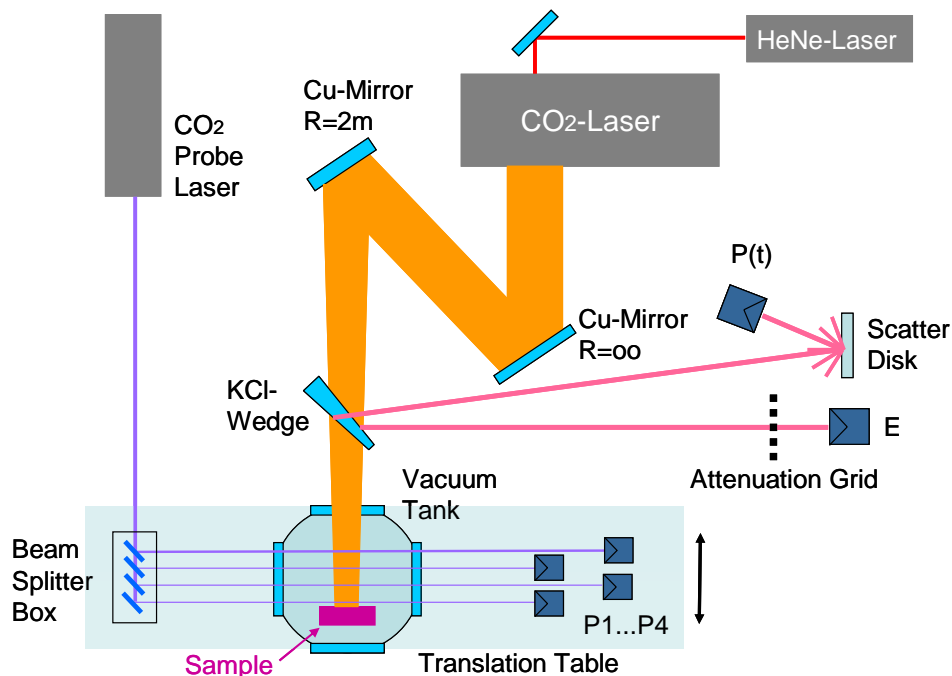


Fig. 3: Initial setup for the absorption measurement with 4 probe beams

The CO₂ probe laser is a product of Ultra Laser Tech and the fast photodetectors are of type PEM-L3 from VIGO. All mirrors and windows were from ZnSe. The detector signal was stored simultaneously with the pulse signal of the CO₂ pulse laser on a digital oscilloscope LeCroy LT 342 with 2000 storage places per trace. The sample rate was 50 MHz with a corresponding time resolution of 20 ns. The beginning of the sampling was triggered by the electromagnetic noise pulse of the spark gap for the ignition of the CO₂ pulse laser. The radiation of the ablation plasma in the CO₂ band could not be eliminated totally and in some

cases was of the same order as the probe laser signal. The result is therefore a superposition of two opposite curves. The plasma radiation signal therefore was always additionally measured with turned off probe laser for later subtraction from the measured curve.

A certain danger for the interpretation of the results was the possibility of a bending of the probe beam out of the detector by strong density gradients. This would pretend an absorption. Therefore, experiments have been carried out with a deliberate offset of the detector from the actual target point. If a bending would have taken place it should have been discovered by an eventual detector signal from the momentarily displaced beam. This did not happen, either because there was no bending or the absorption prevented the signal of a bent beam.

3. RESULTS AND INTERPRETATION

3.1 Energy absorption

Preliminary measurements of the energy transmitted through the absorbing ablation products and the ablation sample via a 3 mm hole on the axis of the pulse laser beam (Ref. 1) have been extended to a broader range of material conditions and pulse energies. The assumption that the initial peak of the power curve after 300 ns is not yet influenced by the absorption mechanism gives the possibility to match the different scales of the power curve of the incident with the transmitted beam. With a sampling interval of 0.01 μs enough data points are available to precisely determine the maximum of the 0.7 μs wide first peak. The integration of both curves yields a non-calibrated, but directly comparable value for the accumulated energy. Therefore, the transmission ratio due to absorption, $R_t = E_{\text{trans}} / E_L$, can be directly inferred. E_{trans} is the energy measured behind the target and E_L is the incident laser pulse energy. The result is plotted in **fig. 4**.

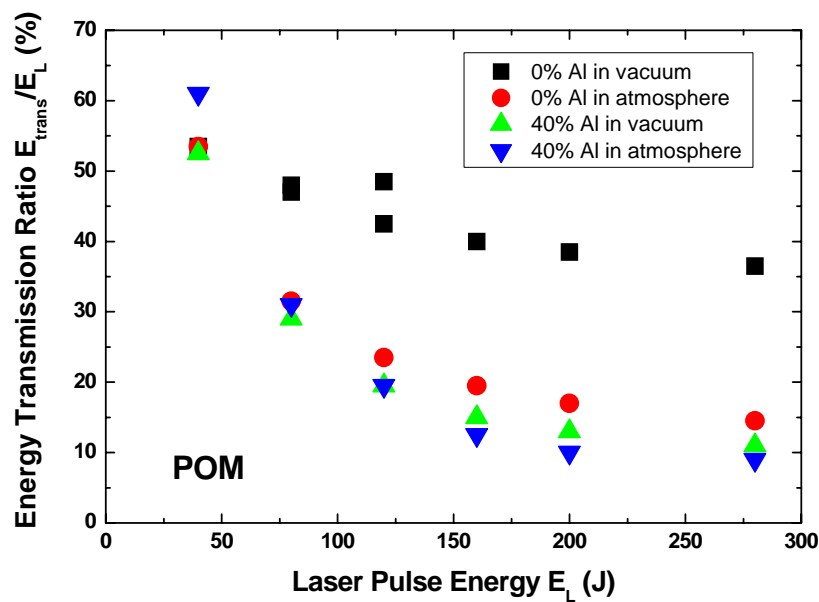


Fig. 4: Fraction of energy transmitted to the target surface

The smoothness of the data course with the laser pulse energy and the scatter of a few repeated measurements gives some confidence into the derived values, in particular with respect to the scale matching of the power curves. It is striking that the ablation of plain POM in vacuum leads to much less absorption (about 35% transmission in the limit of very high

incident pulse energies) compared to the other cases: POM in atmospheric air and POM blended with aluminum powder. In these latter cases less than 10% (!) of the incident pulse energy actually arrive at the target surface in the limit of high pulse energies. A closer inspection of the data course indicates a linear dependence of the transmitted energy ratio R_t on the inverse of the pulse energy E_L . This is shown in **fig. 5**, where the same data are plotted versus $1/E_L$. The approximately matching straight lines can be expressed as

$$\begin{aligned}
 R_t &= 7.167 / E_L + 0.36 && \text{for } 0\% \text{ Al and vacuum} \\
 R_t &= 17.83 / E_L + 0.085 && \text{for } 0\% \text{ Al and atmosphere} \\
 R_t &= 19.5 / E_L + 0.04 && \text{for } 40\% \text{ Al and vacuum} \\
 R_t &= 25.5 / E_L - 0.025 && \text{for } 40\% \text{ Al and atmosphere.}
 \end{aligned}$$

In the limit of large E_L the first term vanishes and the additive term gives the minimum transmission ratio. For large values of E_L however, the last relation is not reasonable, since the transmission ratio cannot become less than zero.

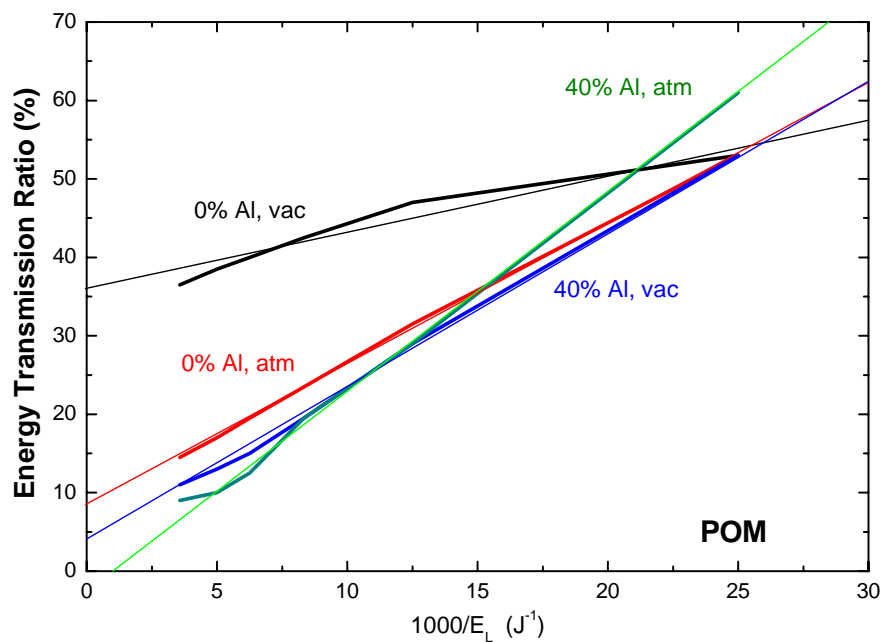


Fig. 5: Correlation of the energy transmission ratio with the incident pulse energy

Another interesting result is the observed shortening of the transmitted laser pulse. It is plotted in **fig. 6** for the same conditions as in the previous diagrams. For POM in vacuum a maximum pulse length is found for the pulse energy of 120 J. The increase in pulse length for lower energies is associated with the general increase of the incident laser pulse length with the pulse energy from about 10 microseconds at the low energies to over 12 μ s at the higher

energies. Above 120 J, the pulse length decreases rapidly, because the effect of pulse shortening by plasma absorption is now taking over. For the other 3 cases the pulse shortening is so strong from the very beginning that no optimum is found anymore. The transmitted pulse duration drops to as low as 1 μs . Finally, only the energy of the initial spike of the power curve arrives at the target.

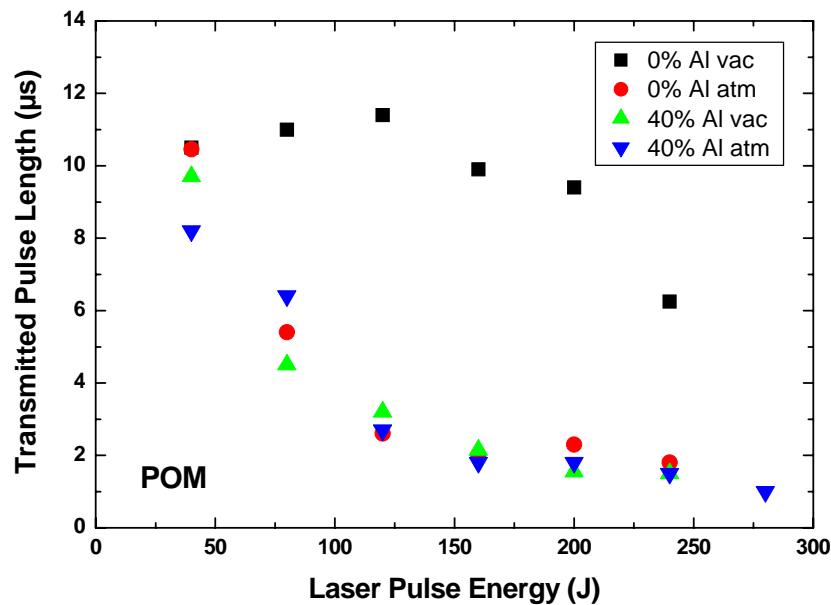


Fig. 6: Length of laser pulse transmitted to the target surface

It may be of academic interest only, but it is still illustrative, to calculate the coupling coefficients that could be achieved if all the energy would arrive at the target and be transformed into a mechanical impulse. Therefore, we have plotted in **fig. 7** values

$$cm_{\text{extrapolated}} = cm_{\text{measured}} / R_t$$

Plotted are only the extrapolated values for plain POM in vacuum and in atmosphere, for which an impulse measurement and a transmission measurement with the same pulse energy has been made. For comparison, the actually measured coupling coefficients are also shown in the diagram with open symbols. The data are taken from ref. 1. An optimum pulse energy is noticed here, too. The theoretically attainable coupling coefficients would reach values as high as 500 N/MW in vacuum and twice this amount in atmospheric air. The result may be an indication for the impulse potential of polymers if the absorption could be suppressed or circumvented by an appropriate laser pulse length.

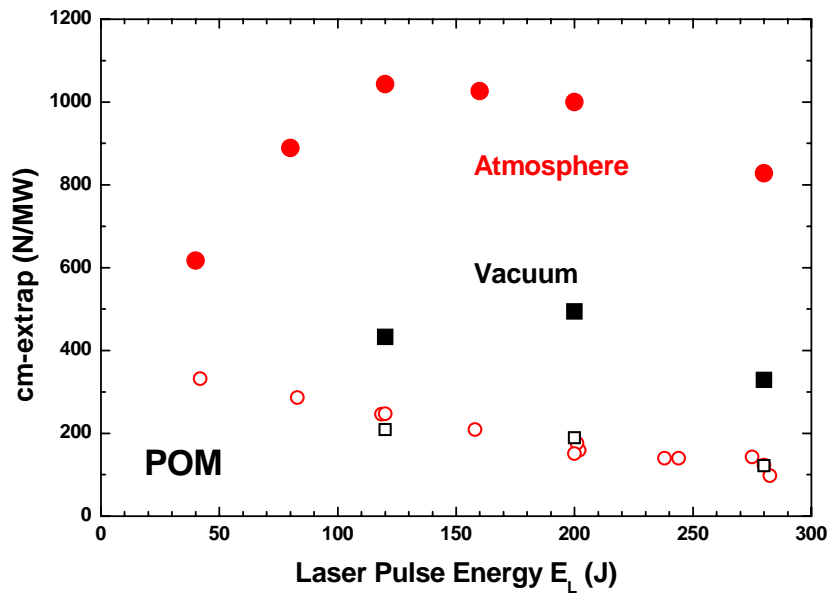


Fig. 7: Comparison of extrapolated potential coupling coefficients for suppressed absorption with actually measured values (open symbols)

3.2 Schlieren photography

Schlieren picture series have been made of plain POM for the following conditions:

| | | |
|------------------|---|----------------------|
| Pressure | below 0.5 mbar, | 35 mbar |
| Pulse energy | 25 J, 75 J, | 150 J |
| corresp. fluence | 13 J/cm ² , 37 J/cm ² , | 75 J/cm ² |

For illustrating the different behavior, a picture series at the same pressures and with pulse energies of 75 J and 150 J has been made for POM with 20% Al also.

Pictures were selected with time delays of approximately 1 μ s separation up to 11 μ s (the end of the laser pulse) after the start of the laser pulse and then after 15 μ s, 20 μ s and 25 μ s.

The picture series are presented in **Appendix A** in two columns with ambient pressure 0 mbar to the left and 35 mbar to the right. Close to the target plane the picture is obscured by the target fixture. Therefore, the plasma development cannot be seen during the first microsecond, corresponding to a maximum distance of \sim 3 mm. The sawtooth like structure at the bottom of

the pictures is the scale with centimeter separation of the kerfs. (The pictures should better be viewed as originals from the screen and not as paper prints to see more details.)

The following general observations can be made:

3.2.1 POM

For both pressures a black ellipsoidal plume develops rapidly and reaches a maximum extension of 10 to 12 mm (energy dependent) after approximately 6 μ s. This is the time when the laser pulse has reached its maximum power, too. Within 1 mm, the extension of the plume is equal for both pressure cases. The black plume is interpreted as the ablation plasma, which has an electron density high enough to absorb the illuminating light. The boundary is of remarkable sharpness. In the low pressure air, the detachment of a spherical shock from the plasma can be seen right after the appearance of the plasma. Several waves and a darker and a brighter zone follow the shock wave at nearly equal distances. The origin of these waves is not known. However, when watching the picture series backwards, it appears likely that the transition from a brighter zone to a darker zone marks the contact front, the boundary between the off-flowing ablation products and the shocked air (darker zone).

When the laser pulse begins to decay after 8 to 9 μ s, the sharp boundary of the plasma decays also and streamers in the flow direction become visible. Prominent vanes appear at the lower and upper boundary of the plasma. These could be artifacts from flow distortions at the screw heads that penetrate into the open space and obstruct a radial expansion. The streamers can be seen even after pulse termination, indicating that a vapor flow from the surface continues for some time, until the sample has cooled enough. After termination of the laser pulse, the contact line also seems to sharpen up. For a pulse energy of 150 J the bright/dark transition disappears after 6 μ s and reappears after 11 μ s. The line has moved out of the field of view after 25 μ s.

3.2.2 POM + 20% Al

A sample with a 20% concentration of aluminum powder has been observed as well. In PVN samples with an additive, Urech et al. have observed a strange phenomenon (ref. 4): The additive seems to expand with a higher velocity and to break through the shock wave. At a first glance this is physically impossible, because the penetrating material would launch another, even faster shock wave into the environment. We wanted to check this observation for our conditions with pulse energies of 75 J and 150 J. In addition, a few samples of plain

PVN, PVN with added Al, and PVN with added C were supplied by Lippert and have been checked as well.

It turned out that we could observe the same phenomenon indeed for the POM sample with Al: At a pulse energy of 75 J the creation of a new, non-uniform cloud is noticed for the first time after 4.7 μs . Already 1 μs later it has reached the initial shock front and after 9 μs it starts to bulge out the shock front. Another 2 μs later it has moved almost twice as far as the initial shock front and an entirely hemispherical front develops. In vacuum, this front can be seen equally well but does show a more irregular shape with local sub-centers. The plasma front is less well defined as in the previous experiments with plain POM and seems to extend not as far as for plain POM. Remarkable is also the disappearance of the Schlieren, at first in vacuum between 11.5 μs and 15.7 μs and thereafter in air, leaving just a diffuse cloud near the target surface with probably still evaporating material. At the pulse energy of 150 J the same phenomenon happens at an earlier time. Already after 3.7 μs the second cloud has reached the shock front and has penetrated through it during the next microsecond. While in the low pressure environment the ejected material remains confined within a sharply bound front, in vacuum it spreads out diffusively in all directions. Apparently, the residual air still exerts a drag force on the ejected matter. In air, the ejection turns into an almost one-dimensional process. Between 8 and 9 μs the ejected matter leaves the field of view.

3.2.3 PVN, PVN + Al, PVN + C

The availability of a few samples of undoped and doped PVN allowed a comparison to other polymers. The few shots that could be made before the samples disintegrated did not uncover any new peculiarities. Note, that even in vacuum a spherical wave can be seen for PVN + C after 3.3 μs . A material penetration through the shock wave has not been noticed.

3.3 Velocity of the ablation products

The series of Schlieren pictures allows the direct measurement of various velocities: shock wave, plasma expansion and with some caution the velocity of the contact front, which would represent the maximum ablation velocity. The data from the pictures have been collected in diagrams of the front positions versus time. These are presented in **figs. 8 – 10** for pure POM and in **figs. 11 and 12** for doped POM and PVN. Also displayed in the diagrams are the

power curves at comparable energetic conditions (the pulse energy for the power curves is given in parenthesis in the legend). The dashed line at 3 mm distance from the target marks the distance, where a feature can be discovered for the first time. The first data point location is therefore not exact and the true location of the surface is not known to better than 1 mm. However, all distances relative to each other are precise to within a fraction of a millimeter. The shock front and the contact front show a linear behavior and thus possess a unique speed for a fixed energy. Yet, the shock speed grows with the pulse energy. But, while the pulse energy is increased 6-fold from 25 J to 150 J, the shock velocity only goes up from 2 km/s to 2.5 km/s. It is not expected that the ablation velocity in vacuum is significantly different from the velocity of the contact front, as interpreted from the pictures in low pressure air. This is very different though for the doped material, for which the ablation products assume a much higher front velocity for the pulse energy of 150 J: over 8 km/s. The few values for PVN are also shown in **fig. 11**. They are not significantly different from the POM values. Locating the material front in vacuum with its chaotic structure is difficult. Therefore, the scatter is much larger. Nevertheless, the data fit with the values in air. The plasma extension is larger and clearly pronounced.

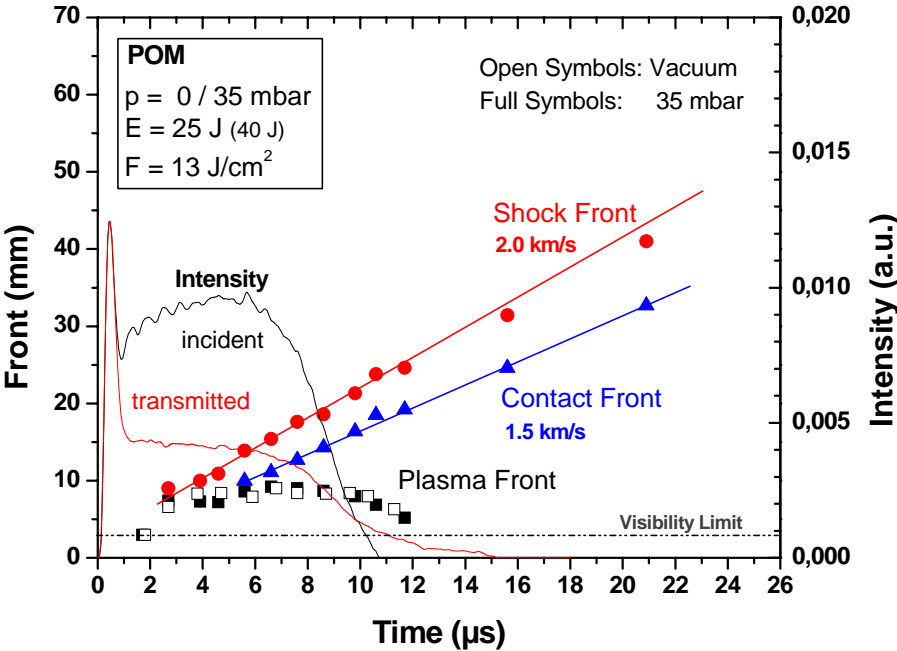


Fig. 8: Space/time diagram of the shock and contact front for a pulse energy of 25 J in comparison with the intensity curve. Target material: POM

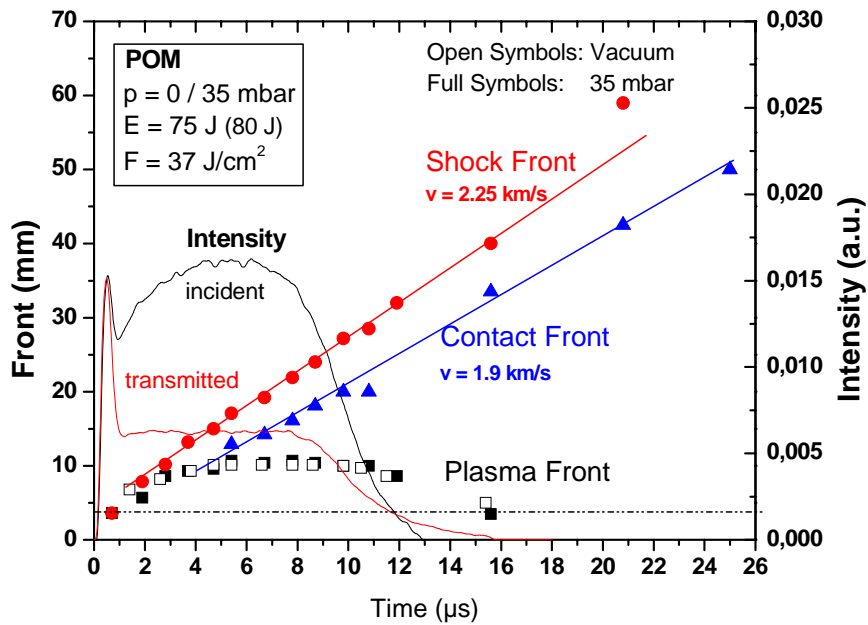


Fig. 9: Space/time diagram of the shock and contact front for a pulse energy of 75 J in comparison with the intensity curve. Target material: POM

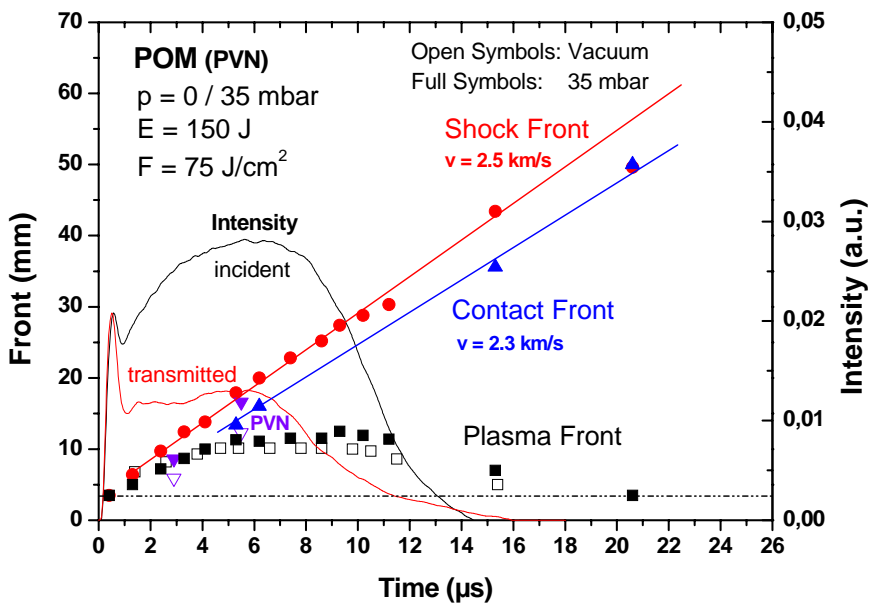


Fig. 10: Space/time diagram of the shock and contact front for a pulse energy of 150 J in comparison with the intensity curve. Target material: POM

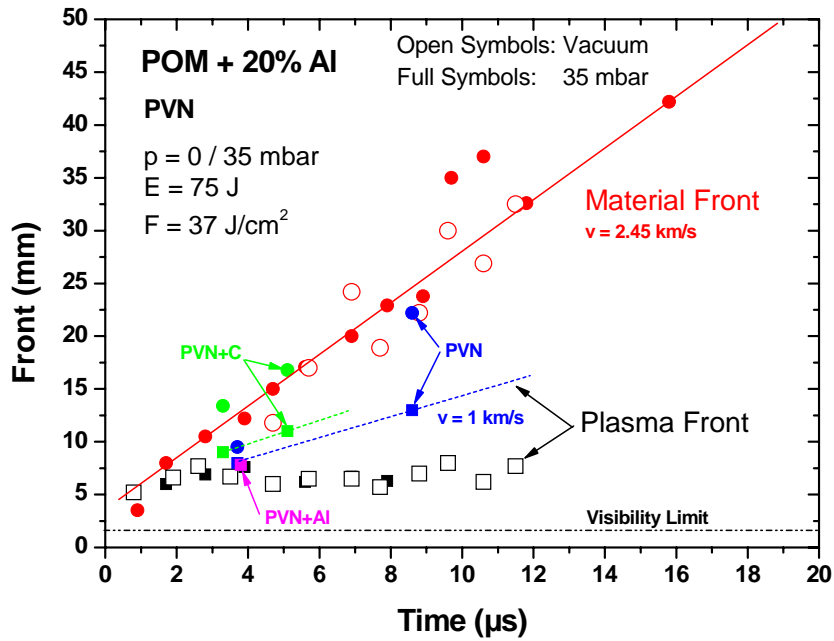


Fig. 11: Space/time diagram of the shock and contact front for a pulse energy of 75 J in comparison with the intensity curve. Target material: POM + 20% Al and PVN

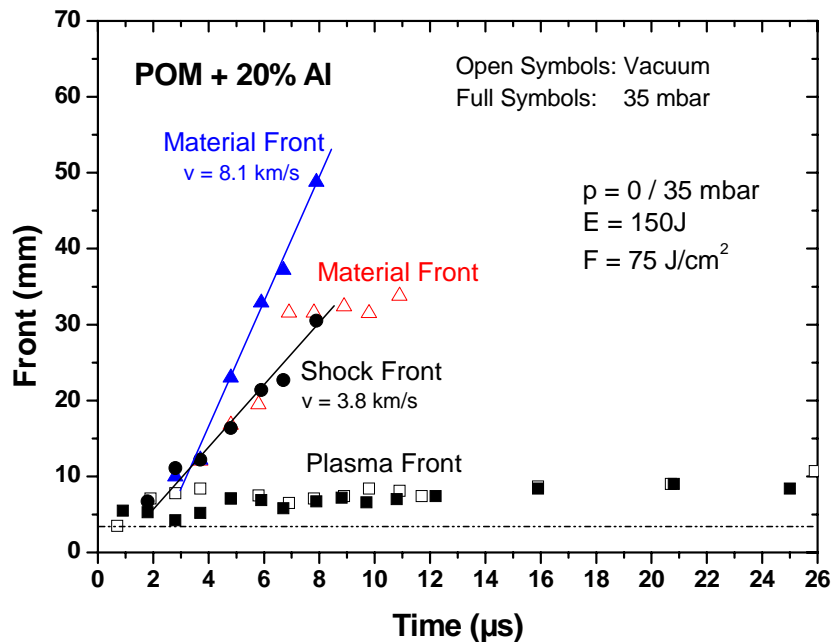


Fig. 12: Space/time diagram of the shock and contact front for a pulse energy of 150 J in comparison with the intensity curve. Target material: POM + 20% Al

It is surprising that the velocities of the shock and contact front are constant over time. This is expected for a one-dimensional expansion only. For multi-dimensional expansion one would expect a slow-down of the velocity with time, because the driving energy dissipates in several directions. If one assumes the expansion being one-dimensional, and the shock velocity in a gas of known thermodynamic state is also known, one can use the shock formulas to get an idea about the motion of the gases behind the shock wave. If the gases are thermally perfect, the pressure and the temperature jump across the shock wave are expressed as

$$\frac{p_2}{p_1} = 1 + \frac{2\gamma}{\gamma+1} (M_1^2 - 1)$$

$$\frac{T_2}{T_1} = 1 + \frac{2(\gamma-1)}{(\gamma+1)^2} \frac{\gamma M_1^2 + 1}{M_1^2} (M_1^2 - 1)$$

The indices correspond to the undisturbed gas, 1, and the gas behind the shock front, 2. M_1 is the Mach number of the shock wave with respect to the ambient gas and γ is the isentropic coefficient of the gas. The velocity of the gas behind the shock wave relative to its motion is given by

$$v_2^2 = \frac{1}{2\rho_1} \frac{[(\gamma+1)p_1 + (\gamma-1)p_2]^2}{(\gamma-1)p_1 + (\gamma+1)p_2}$$

ρ_1 is the density of the undisturbed gas. The absolute flow velocity of the shocked gas is

$$u = v_1 - v_2$$

This is also the velocity of the contact front and hence of the ablation products. For air at room temperature and a pressure of 35 mbar, **table 1** gives the conditions for the measured shock waves. Note, that these are only theoretical values, because for the high temperatures behind the shock the air is no more ideal.

Table 1. Results for a 1-dimensional shock wave

| E_L (J) | v_1 (m/s) | M_1 | u (m/s) | P_2 (bar) | T_2 (K) |
|----------------------------------|-------------|-------|-----------|-------------|-----------|
| <u>$\gamma = 1.3$</u> | | | | | |
| 25 | 2000 | 5.83 | 1699 | 1.34 | 1752 |
| 75 | 2250 | 6.56 | 1923 | 1.70 | 2142 |
| 150 | 2500 | 7.29 | 2146 | 2.10 | 2578 |
| <u>$\gamma = 1.4$</u> | | | | | |
| 25 | 2000 | 5.83 | 1618 | 1.38 | 2213 |
| 75 | 2250 | 6.56 | 1831 | 1.75 | 2728 |
| 150 | 2500 | 7.29 | 2044 | 2.16 | 3304 |

The measured velocities of the potential contact surface are 1500; 1925; and 2275 m/s. As the pulse energy is increased, the isentropic coefficient should be reduced to less than 1.3, which seems reasonable. It is remarkable that the pressure behind the shock wave in the disturbed air rises to over 1 bar and the temperatures reach values up to 2500 K.

While in the case of plain POM the radiation penetrates into the material according to the optical transmission, decomposes the chemical structure, and vaporizes the products, it is conceivable that with the larger concentrations of optically dense materials, like metals a different process takes place. One explanation could be that the metal grains act as scattering objects that guide light to some depth. Interference may lead to local energy concentrations. The polymer with its low decomposition temperature goes into a gaseous state and builds up a pressure that is finally capable to eject the metal grains with very high speed like in a cannon. This process would have some similarity with a confined ablation (refs. 5 and 6).

3.4 Results of the absorption measurements

With the setup, described in Sec. 2.2, it was possible to scan the zone for 10.6 μm absorption in front of the target and look at the temporal development of the absorption fraction. Two major problems made the evaluation of the measurements difficult: 1) The continuous plasma radiation was very strong around the CO_2 band compared to the probe laser beam intensity and could not be totally suppressed. However, increasing the distance of the powermeter from the radiation source reduced the background to an acceptable level. The signal was still very noisy. 2) As the probe beam is moved away from the sample surface and due to the finite expansion velocity of the ablation cloud, the onset of absorption must be delayed in proportion to the distance. This was the case in general. Surprisingly, for a certain percentage of measurements the absorption started right after the ablation laser pulse, even at distances as far away as 16 mm. The phenomenon of occasional early absorption could not be clarified during the campaign of the absorption measurements. A series of control measurements have been made to find out possible effects that could lead to a premature absorption. Details are discussed in Sec. 3.5. In the following we will describe the results considered to be regular. Absorption measurements were carried out for pulse energies of 150 J, 75 J and 25 J in vacuum and also for 150 J in ambient air of 30 mbar.

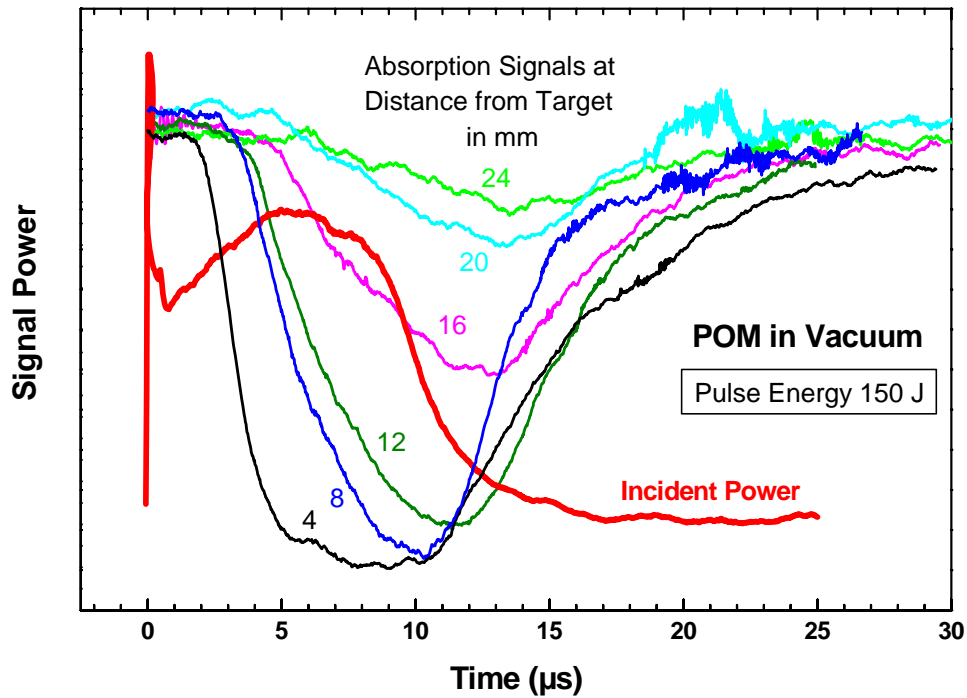


Fig. 13: Temporal development of the CO₂ wavelength absorption at various distances from target surface for a pulse energy of 150 J

Because of the strong noise of the absorption curves the following procedure was necessary to produce the results: First the curves were smoothed out on the computer by a conventional smoothing routine. Then five curves of equal conditions were superimposed to artificially raise the intensity. From the resulting curve the signal without the probe beam, comprising the plasma radiation in the observed wavelength band and some possible stray light, was subtracted from the probe beam signals.

As a function of time after the beginning of the laser pulse, **fig. 13** shows the power traces of the partially absorbed probe beam for various distances from the target surface. For comparison, the power trace of the pulse of the ablation laser is also included in the diagram ("incident power"). The measurements shown in this diagram have been made for POM in vacuum with a pulse energy of 150 J. The resolution in location is comparable to the diameter of the probe beam at the location of the measurement. For the presented results this is 2 mm. Due to the finite angular resolution of the setup, plasma radiation from upstream regions may be seen before absorbing media cross the probe beam. The absorption is strongest near the target and decreases with the distance. The absorption also lives longest near the target where

plasma recombination is delayed by lasting high temperatures. **Fig. 14** is a 3-D re-plot of the absorption region in space and time, with the absorption strength in vertical direction. Note: The magnitude of the absorption for different time traces is arbitrary. The diagrams are only to show the extension and motion of the absorption region in the space-time domain.

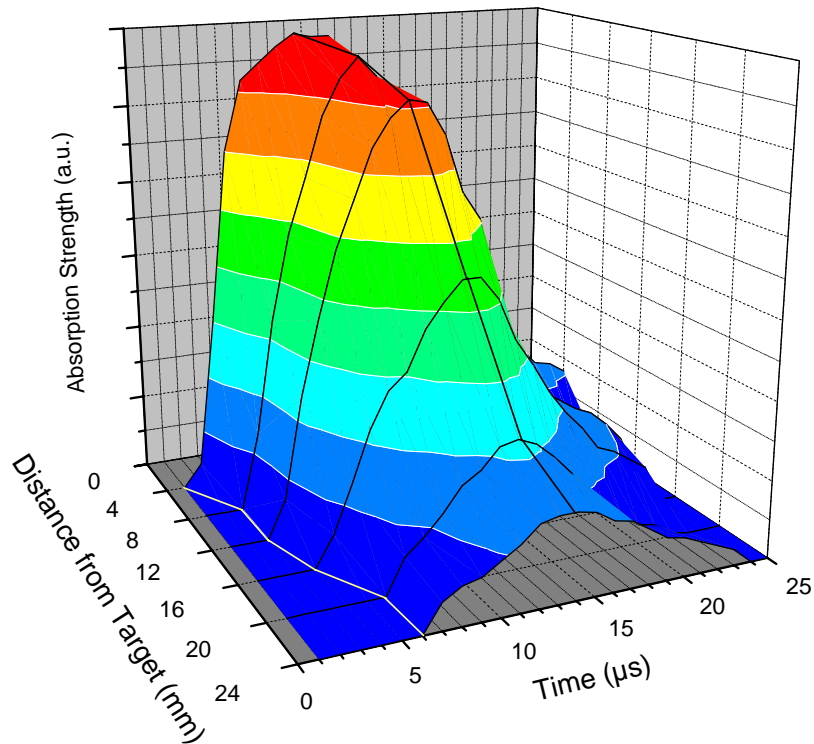


Fig. 14: 3-dimensional representation of the absorption wave

The spreading velocity of the absorption wave can now be deduced from the data. **Fig. 15**, for instance, is a plot of the time delay of the onset of absorption and of the absorption maximum versus the distance from the sample surface. **Fig. 16** shows the respective velocities, calculated from the space/time curve. In order to reduce the error in the derivative of the data of **fig. 15**, the measured data have been corrected by an idealized hand fit, as shown by the superimposed lines in **fig. 15**.

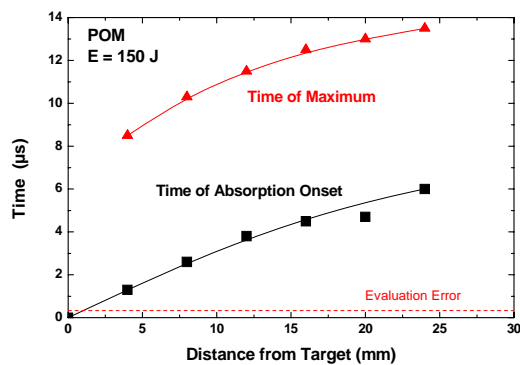


Fig. 15: Time of the onset and the maximum of the absorption wave

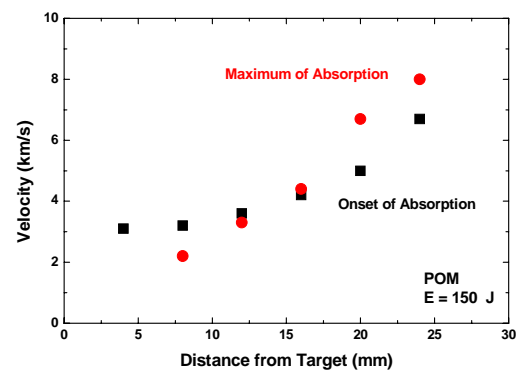


Fig. 16: Velocities of the absorption wave

The surprising result of these measurements is (1) the high, and (2) an even strongly accelerating velocity of both, the onset of the absorption (> 3 km/s) and the attaining of the absorption maximum (> 2 km/s). The result does not correspond to the findings with the Schlieren observations, where a constant material velocity (contact front) of 2.3 km/s to distances of 50 mm from the target has been found (**Fig. 10**). Absorbing matter would have to expand much faster than can be seen in the Schlieren pictures. What kind of matter could that be and where does it come from? Is there a connection to the onset of an abnormal absorption? If some available matter is postulated, at least the increasing acceleration could be explained in terms of a detonation wave with a constant heating in the region immediately behind the front. But a detonation wave, precursing the shock wave should be visible in the Schlieren pictures.

A fundamental difference of the absorption measurements is the lack of ambient low pressure air that was helpful for the interpretation of the Schlieren pictures. If in the case with a low background pressure the absorption wave speed is comparable to the shock wave, then we can conclude that in vacuum some matter escapes with the absorption wave speed indeed and a detonation front remains just invisible because of the very low pressure. In this case the Schlieren pictures would not be representative for the development of absorption in vacuum. This has been tested by comparative absorption measurements with the same pulse energy of 150 J, but with a background pressure of 30 mbar air. The resulting absorption curves are shown in **fig. 17**.

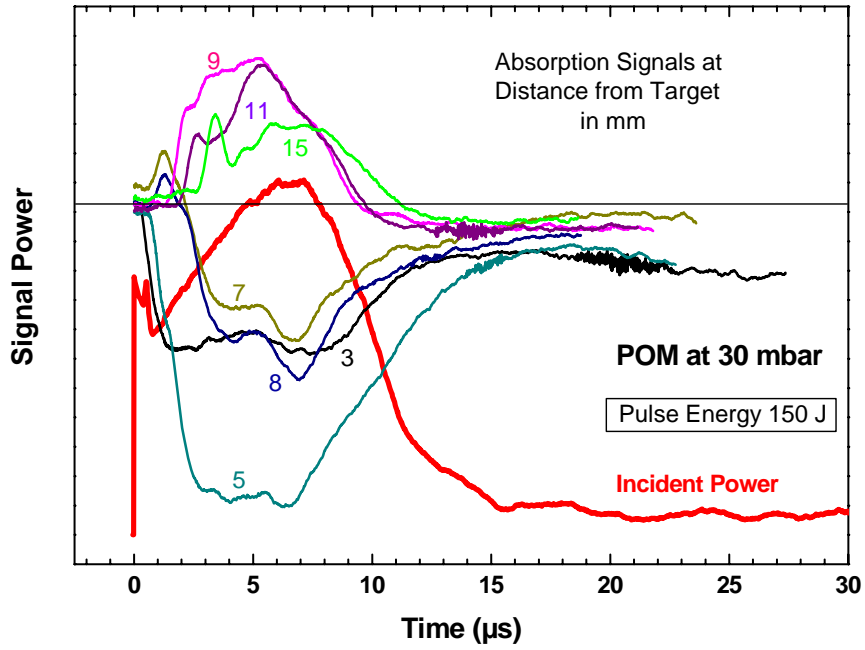


Fig. 17: Temporal development of the absorption wave, when a low pressure background gas (air at 30 mbar) is present

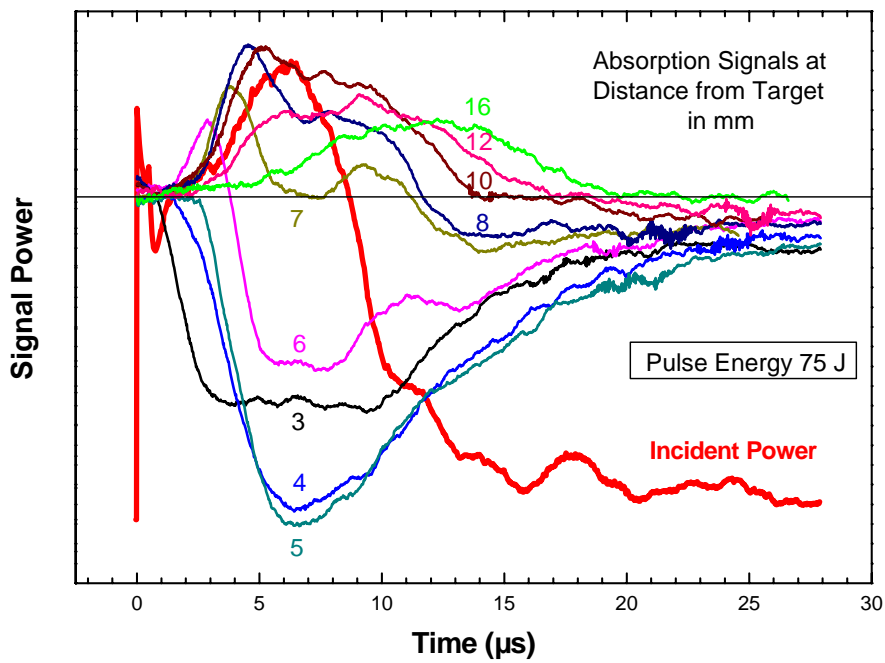


Fig. 18: Temporal behavior of the absorption in vacuum for a pulse energy of 75 J

In addition to absorption measurements at 150 J, comparable measurements have been made for lower energies in order to see the influence of the energy in the plasma on the absorption velocity. Measurements at a pulse energy as low as 25 J did not result in any measurable change of the probe beam intensity. Thus, absorption is insignificant at such low energies, respectively flux and intensities. This result is not unexpected in the light of the high energy fraction that arrives at the target, as suggested from **fig. 4**. The results from a measurement at a pulse energy of 75 J, however, are shown in **fig. 18**. **Figs. 17 and 18** show a distinctive difference to **fig. 13**. Absorption curves for distances greater than 5 mm from the target show an initial positive peak before they become negative or they even remain positive for all the time. This seemingly strange behaviour is an artifact that is produced when the plasma signal and the absorption become of the same magnitude. If the absorption then lags somewhat behind the plasma signal, the initially positive peak appears. The various possible cases of the addition of two oppositely running curves are formally described in **Appendix B**. In such cases the first peak marks the onset of absorption.

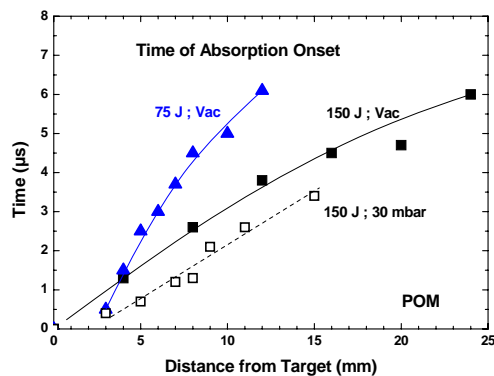


Fig. 19: Time of the onset of absorption for different conditions

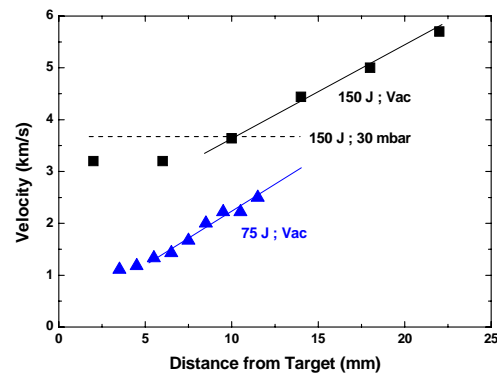


Fig. 20: Spreading velocity of the absorption wave

In **figs. 19 and 20** the space/time correlation and the derived velocities for the onset of absorption for the new conditions are compared with the case of 150 J in vacuum. A shift of the onset of the curves in distance from the target by 2.5 to 3 mm is probably a systematic error in relating the probe beam to the target surface and is not considered of importance. Again the velocities are derived from the differentiation of the idealized space/time curve, shown by the associated lines. The values for 150 J in a 30 mbar air environment can be approximated by a straight line and yield a velocity of 3.7 km/s, which is in rough agreement with the values found for vacuum. Again the velocity is considerably higher as derived from the Schlieren pictures. In the case of 75 J the velocity of the absorption onset is substantially

lower as for the double energy. It starts out with about 1 km/s and begins to accelerate with the same rate as in the case of 150 J. The corresponding (constant) contact velocity from the Schlieren pictures is 1.9 km/s. As this velocity is only reached at a distance of about 8 mm, it suprisingly appears that there is no connection between the results from the two methods. Therefore, it must be concluded that the nature of the absorbing media remains in the dark!

3.5 Abnormal absorption

Abnormal absorption is understood as the absorption that starts immediately with the laser pulse. **Fig. 21** gives an example of a normal and an abnormal absorption curve for the same conditions. We have attempted to find the reason for this as yet unidentified phenomenon by procedures described below. The only natural explanation is a breakdown independent of the target. Such a breakdown can happen in a gas with a low breakdown threshold, for instance in residual air, possibly contaminated with products of the previous ablation shot. Although the vacuum pump is running continuously, this seems conceivable, if some dust that has settled down on the tank wall is whirled up again by an ablation shot. Also, floating dust may not settle down for a long time. In addition, the local intensity in front of the target may be enhanced by reflections from the target. The hypothesis that residual air might trigger a premature breakdown is not supported though by the measurements with 30 mbars of background air. No early breakdown was found in these measurements.

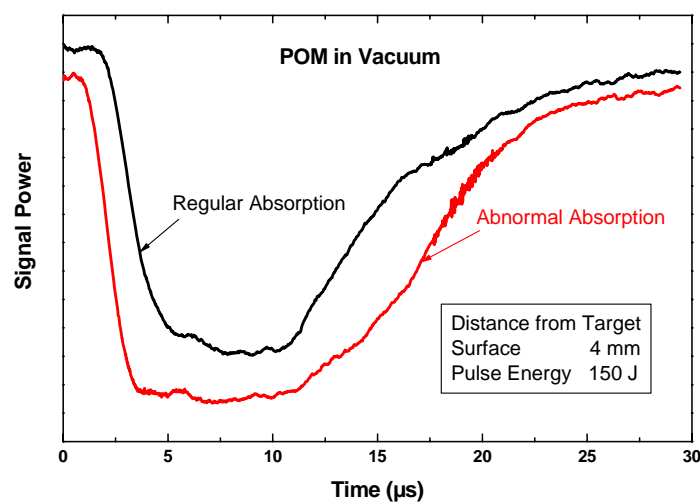


Fig. 21: Comparison of the abnormal absorption with the regular case

Nevertheless, a series of individual tests have been performed to rule out more or less obvious causes. For these tests, the probe beam was placed 6 mm in front of the target. The pulse energy was always kept at 150 J. Some of the results are displayed in **Fig. 22**.

- 1) The presence of residual air or other contamination products has been reduced by extended pumping before the next shot (1/2 hour with a final pressure < 0.05 mbar). Abnormal absorption was observed anyway (Diagram 19, curve # 4).
- 2) Careful cleaning of the tank and purging with dry nitrogen did not prevent the abnormal absorption.
- 3) Artificial contamination has been attempted by blowing nitrogen across the target surface. This raised also the pressure in the tank. The abnormal absorption was not enforced.
- 4) Puffs of gas into the tank before a shot to whirl up any settled down contamination did not result in abnormal absorption (curve # 2).
- 5) Continuous flushing at a distance of 5 cm from the target surface (curve # 1) and at 1 cm (curve # 3) gave ambiguous results.
- 6) After the complete removal of target and target holder no absorption was found at all.

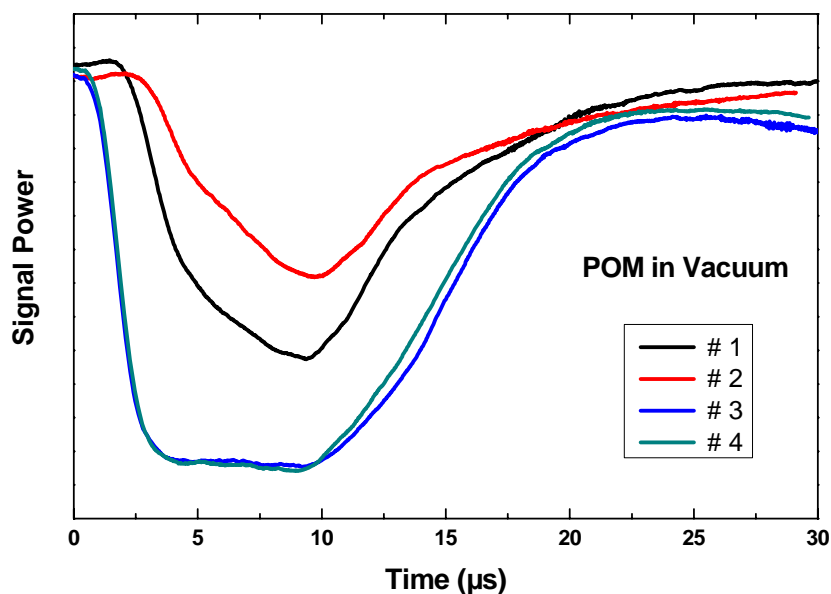


Fig. 22: Comparison of normal and abnormal absorption curves for different experimental conditions. (# 1: continuous flushing 5 cm from sample surface; # 2: flushing 5 cm from sample surface, then pulse after some delay; # 3: continuous flushing 1 cm from sample surface; # 4: no flushing, pressure < 0.05 mbar)

- 7) Replacing the polymer target by a target of sandblasted aluminum resulted in a very bright plasma and an initially strong absorption. This absorption, however, decreased with every consecutive shot and is thus contributed to surface contamination of the sample.
- 8) The effect of a deflection of the probe beam by the expanding gas has been checked once more and none was found.
- 9) A possible interference of electromagnetic radiation with the detector has been ruled out by successively covering up all optical radiation.
- 10) In the same way, scattering by secondary reflections of the ablation laser pulse into the detector has been ruled out.
- 11) Finally, it has been checked if the laser emits a prepulse that had remained undetected by the applied trigger method. No such pulse was found that could have released a small amount of matter from target before the main pulse was applied.

All these tests led to no concise conclusion on the origin of the abnormal absorption and how to prevent it. Other explanations, like very fast precursor electrons from the target plasma, can probably be ruled out because of the build-up of a space charge. But the ions would follow not faster than the shock wave expands and hold the electrons back. Also, such a process should occur for every shot.

4. CONCLUSION

It was found that the fraction of energy that is not absorbed in front of the target surface is inversely proportional to the applied pulse energy. The length of the penetrating energy pulse is also shortened with increasing pulse energy. In the limit, only the initial spike energy can penetrate to the target surface.

In the experiments employing Schlieren Photography with nanosecond exposure times we could show the formation of a surface plasma along with the deposition of energy into a target sample. The plasma expands to a maximum distance of 12 mm from the surface. In a gaseous environment the plasma expansion launches a strong shock wave with Mach no. ~ 6 . From the velocity of the shock wave and the assumption of a quasi one-dimensional expansion process, an approximate expansion velocity of the material cloud of ablation products can be deduced. As the released gas or vapor expands, an absorption wave spreads out. This is, where most of the incident pulse power is subsequently absorbed. The addition of heat into the off-flowing matter can be one reason why the velocity, observed as the shock velocity, does not decrease over an extended time, as would be expected for a multi-dimensional expansion. The circular shape of the density gradients, as seen in the Schlieren pictures, does suggest a 3-dimensional expansion, although probably not in the full half-space. Shock velocities in the range of the applied pulse energies of 150 J (fluence 75 J/cm^2) were not higher than 2.5 km/s for plain POM. Only POM samples blended with a certain amount of metal powder showed an unusual behavior with material escape velocities in excess of 8 km/s. Since such high material speeds did not result in improved generation of the mechanical impulse, this very interesting finding deserves some more investigations of fundamental nature.

Position and time resolved measurements of the absorption cloud itself have been made in the same parameter regime as the optical Schlieren observations, using a CO_2 probe laser beam transversely through the expanding cloud. Surprisingly, the measured absorption wave generally expands much faster than the optically measured velocity of the shock wave. Furthermore, the velocity of the onset of absorption increases in time at a constant rate. No correspondence between the material expansion and the absorption wave could be made out. Also a nearly instantaneous absorption has been observed occasionally. These effects prompted a series of different tests to rule out influences from unclean experimental conditions. No situation was found that could yield the described effects. We are left with the

unsatisfactory circumstances that two processes have been observed with different expansion behaviour that could not be brought into an at least close agreement. The explanation for the absorption, which is so important for the achievement of high impulses in ablation propulsion, thus remains still an open question.

It had been claimed that the applied CO₂-laser pulse, consisting of two peaks, simulates a double pulse arrangement. In the double pulse arrangement a first pulse releases some matter from the target into which a second, stronger pulse is placed. The resulting shock wave that travels backwards towards the target should give rise to a pressure jump and hence an impulse at the target surface. However, the Schlieren pictures show a fairly continuous motion in one direction only. There is no indication of a wave travelling backwards towards the target surface. Therefore, no retrograde build-up of pressure is expected as a result of a second shock wave. The application of the double pulse effect would require two independent pulses, in which the heating process from the first pulse is completely terminated before the second pulse arrives.

In summary, we must conclude from the results, that a CO₂ laser with pulse lengths of several microseconds in combination with polymers as propellant is not an ideal laser for beamed energy propulsion. The pulse length should be much shorter than the characteristic time for the build-up of an absorption wave, which is less than 1 μs. Energy that is absorbed in such an absorption zone serves only to increase the expansion rate of the zone itself and has no effect back on the target. Pulsed laser ablation rockets, that gain their momentum only from the release of matter directly at the target surface probably work only efficiently for either low energy pulses at a relatively high pulse rate (kHz) or with sub-microsecond pulse lengths. For pulsed high-power CO₂ lasers these conditions are not easy to achieve and require special development efforts.

Unfortunately, the true nature of the absorbing media could not be unveiled, since no coincidence between the absorption measurements and the flow visualisation could be made out. It was the promise that the knowledge about the absorption mechanism could lead to a design where the absorbing medium can be confined in some kind of thrust chamber, like those of conventional rockets. Then, a pressure would build up and produce an additional momentum. In the limit this would lead to the continuous laser rocket. Now, future research

with new methods of investigation must lead to a better understanding of the absorption phenomenon and its coupling to the ablation process.

Acknowledgements

The authors are grateful to Dr. Franklin Mead, Dr. Carl W. Larson and Dr. Ingrid Wysong for the initial support of this project. We also thank Dr. Thomas Lippert for interesting discussions and the supply of samples of new polymer compounds. Finally, we acknowledge the periodic support in the experiments by Sebastian Walther.

LITERATURE

1. W.O.Schall, H.-A.Eckel, J.Tegel, F.Waiblinger, S.Walther, "Properties of Laser Ablation Products of Delrin with CO2 Laser", EOARD Grant FA8655-03-1-3061, Final Report, May 2004.
2. C.R.Phipps and J.Luke, "Micro Laser Plasma Thrusters for Small Satellites", High Power Laser Ablation III, Proc. of SPIE Vol. 4065 (2000) p.801-809.
3. D.A.Reilly, "Laser Propulsion Experiments - Final Report", AVCO Research Lab, Inc., Everett, Maine 02149, Subcontract B116822 for University of California Livermore National Laboratory, Jordan Kare, Program Manager (1991).
4. L.Urech, M.Hauer, T.Lippert, C.R.Phipps, E.Schmid, A.Wokaun, I.Wysong, "Designed polymers for laser-based microthrusters – correlation of thrust with material, plasma, and shockwave properties", High Power Laser Ablation V, Proc. of SPIE Vol. 5448 (2004) p.52-64.
5. K.Mori, K.Watanabe, A.Sasoh, "Large impulse launch using 300-J CO2 TEA Laser", Beamed Energy Propulsion: Third International Symposium on Beamed Energy Propulsion, American Institute of Physics Conference Proc. 766 (2005) p.385-393.
6. R.Fabbro, J.Fournier, P.Ballard, D.Devaux, J.Virmont, "Physical study of laser produced plasma in confined geometry", J.Appl.Phys. Vol.68, No.2 (1990) p.775-784.